

Improved Semantic Segmentation from Ultra-Low-Resolution RGB Images Applied to Privacy-Preserving Object-Goal Navigation

Xuying Huang

Sicong Pan

Olga Zatsarynna

Juergen Gall

Maren Bennewitz

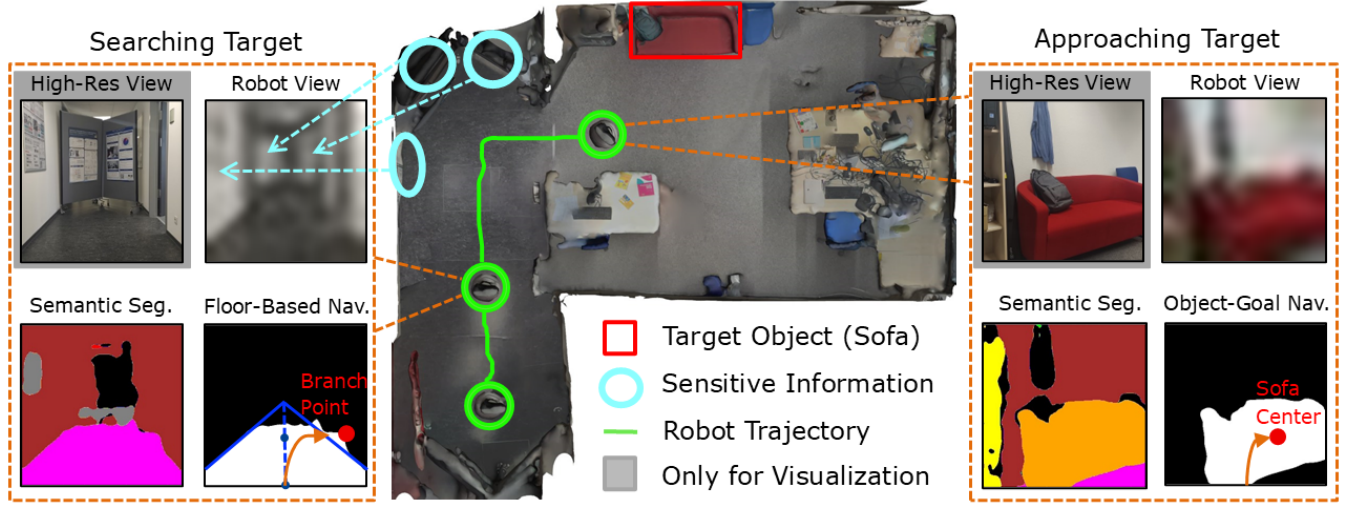


Fig. 1: Our key innovation lies in enabling object-goal navigation through improved semantic segmentation from ultra-low-resolution RGB inputs, thus preserving privacy while maintaining functionality. This figure shows an example of privacy-preserving object-goal navigation using our approach. The High-Res Views show full-resolution RGB images for visualization only, while the Robot Views display the actual robot input: ultra-low-resolution (16×16) monocular RGB images. Cyan dashed lines indicate that sensitive information is effectively concealed due to the ultra-low-resolution input. On the left, when the target object has not yet been found, the robot performs floor-based navigation by following waypoints (blue dots) along the floor centerline (blue dashed line), turning at branch points that may lead to new rooms. On the right, once the target object has been detected, the robot switches to object-goal navigation, gradually approaching the object's center. As can be seen, our pipeline achieves improved semantic segmentation from ultra-low-resolution RGB images.

Abstract—User privacy in mobile robotics has become a critical concern. Existing methods typically prioritize either the performance of downstream robotic tasks or privacy protection, with the latter often constraining the effectiveness of task execution. To jointly address both objectives, we study semantic-based robot navigation in an ultra-low-resolution setting to preserve visual privacy. A key challenge in such scenarios is recovering semantic segmentation from ultra-low-resolution RGB images. In this work, we introduce a novel fully joint-learning method that integrates an agglomerative feature extractor and a segmentation-aware discriminator to solve ultra-low-resolution semantic segmentation, thereby enabling privacy-preserving, semantic object-goal navigation. Our method outperforms different baselines on ultra-low-resolution semantic segmentation and our improved segmentation results increase the success rate of the semantic object-goal navigation in a real-world privacy-constrained scenario.

I. INTRODUCTION

With the widespread deployment of mobile robots in daily life, user privacy has become an increasing concern. When operating in private environments, robots may inadvertently capture sensitive user data through their onboard cameras, such as identification numbers, human faces, or medical records. To mitigate privacy concerns, prior work has explored the use of alternative image modalities, such as depth and semantic segmentation images [11, 14], to generate privacy-preserving representations for diverse downstream robotic applications.

To obtain semantic segmentation images for robotic tasks, high-resolution (HR) RGB images are often indispensable [1, 14, 25]. However, HR images inherently contain rich semantic details, which raise privacy risks [5]. To address this, another line of work investigates directly using low-resolution (LR) RGB images (15×15) [8]. These LR inputs are then used exclusively for privacy-preserving sparse mapping. Nevertheless, LR images convey very limited semantic information, which limits downstream robotic applications, as many tasks require access to depth or semantic information. Therefore, we propose a novel pipeline that uses LR

X. Huang, S. Pan and M. Bennewitz are with the Humanoid Robots Lab, O. Zatsarynna and J. Gall are with Computer Vision Group at the University of Bonn, Germany. X. Huang, S. Pan, J. Gall and M. Bennewitz are additionally with the Lamarr Institute for Machine Learning and Artificial Intelligence and the Center for Robotics, Bonn, Germany. This work has been partially funded by the BMBF, grant No. 16KIS1949 and within the Robotics Institute Germany, grant No. 16ME0999. Corresponding: huang@cs.uni-bonn.de.

RGB images to generate improved semantic segmentation maps, thereby enabling privacy-preserving, segmentation-based robotic tasks, such as object-goal navigation [26].

To investigate the relationship between the resolution threshold of RGB images and privacy, we follow the results of the user study by Huang *et al.* [7]. RGB images with a resolution of 32×32 are generally considered acceptable by users, while resolutions of 16×16 or lower are deemed necessary to fully ensure privacy. In this work, we define such extremely LR inputs (i.e., 16×16) as ultra-low-resolution (ULR), and focus on only utilizing them to generate improved semantic segmentation, as they are considered sufficient to fully preserve user privacy.

In ULR RGB images, visual information is severely limited, which hinders the performance of semantic segmentation. A natural solution is to leverage priors from super-resolution (SR) methods to recover semantic segmentation from ULR inputs. However, existing approaches consistently fail to achieve satisfactory segmentation performance, whether through directly applying pretrained SR models [3], training only the SR [6] or segmentation branch, or even employing end-to-end joint learning [13]. To address these limitations, we introduce a novel joint-learning framework that incorporates a segmentation-aware discriminator and an agglomerative feature extractor, enabling effective recovery of improved semantic segmentation from ULR RGB images.

To the best of our knowledge, we are the first to achieve recovering improved semantic segmentation from ULR RGB inputs for privacy-preserving, semantic-based robotic tasks. Fig. 1 illustrates the application and functionality of our system. For simplicity, we refer to our pipeline that recovers high-quality semantic segmentation from ULR RGB images as ULR semantic segmentation. To summarize, our contributions are the following:

- We develop a novel joint-learning architecture integrating an agglomerative feature extractor and segmentation-aware discriminator, which outperforms different types of strong baselines on the SUN RGB-D dataset [20] as well as our real-world custom dataset on ULR semantic segmentation.
- We provide further analysis to explain why super-resolution modules in existing baselines do not directly improve ULR semantic segmentation, supported by additional super-resolved evaluation metrics.
- We show that our improved ULR semantic segmentation results increase the success rate of the semantic object-goal navigation in a real-world privacy-constrained scenario.

To support reproducibility and future research, our implementation will be made open-source at: <https://github.com/hxy-0818/ULR2SS>.

II. RELATED WORK

In this section, we first introduce relevant work on user privacy in mobile robots and, afterwards, approaches to LR semantic segmentation.

A. User Privacy in Mobile Robots

As mobile robots become growing prevalent in everyday life, user privacy in robotic applications has received increasingly attention [17]. Early work by Reinhardt *et al.* [16] introduce a comprehensive taxonomy of privacy dimensions, i.e., informational, physical, psychological, and social privacy to characterize the risks posed when robots collect and process data during operation. Vision sensors, particularly HR RGB cameras, have emerged as a primary vector for informational privacy violations in robotic applications [23]. Such cameras capture fine-grained textures that enable inference of facial identity, license plates, textual identifiers, and even emotional states. To mitigate the informational privacy risks inherent in HR robotic vision, several studies have investigated leveraging alternative image modalities to support privacy-preserving robotic downstream tasks. For example, MOSAIC [11] introduces a diffusion-based framework that entirely removes RGB inputs, generating consistent and privacy-preserving indoor scenes from multiple depth views. SegLoc [14] constructs compact 3D maps from semantic segmentation labels to enable privacy-preserving visual localization. However, this method depends on HR RGB inputs to generate improved semantic segmentation, thereby necessitating the capture of detailed visual data and perpetuating user privacy concerns [7].

Another line of work is to enforce privacy at capture time by directly reducing the resolution of RGB images from the source. [8] captures RGB images of 15×15 resolution and achieves privacy-preserving sparse mapping solely from such ULR RGB inputs. While this approach relies solely on ULR RGB inputs to protect privacy, its applicability in robotics is limited, as most tasks demand depth or semantic information.

To address the limitations of semantic representations and ULR, we introduce a novel pipeline that reconstructs improved semantic segmentation from ULR RGB images and subsequently drives privacy-preserving, segmentation-based robotic tasks.

B. Low-Resolution Semantic Segmentation

The problem of recovering semantic segmentation from LR RGB inputs has been studied before. For example a common paradigm pretrained pipeline [3] leverages a pretrained SR model to first enlarge the LR images and then applies a pretrained segmentation network.

Beyond the direct use of pre-trained networks, some work has explored monomodule training methods, which train the SR or segmentation network to improve segmentation performance in remote sensing imagery. [6] freeze a pre-trained segmentation model to serve purely as a feature extractor while training only the SR network, whereas another alternative [13] is to first upscale the LR RGB input, e.g., using bicubic interpolation and then train solely the segmentation model.

As an alternative, [13] also investigates adopting a fully joint-learning strategy, in which a single end-to-end pipeline simultaneously optimizes SR and semantic segmentation objectives. Although fully joint-learning approaches achieve

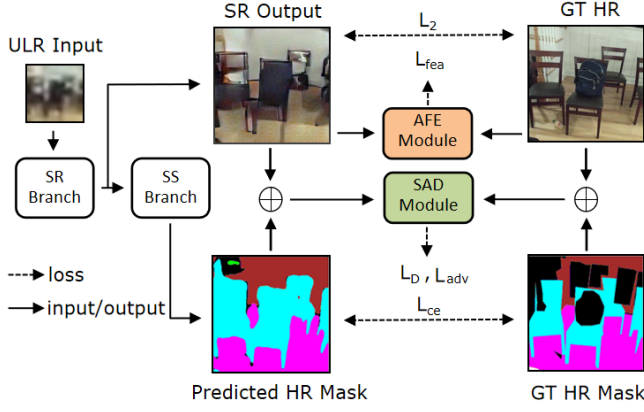


Fig. 2: Overview of our proposed joint-learning framework for ultra-low-resolution semantic segmentation. SS represents semantic segmentation. Given an ULR RGB image, we leverage a GAN-based SR model to generate HR RGB. The super-resolved image is then fed into a semantic segmentation network, which produces a predicted semantic map. We integrate a AFE module to extract high-level semantic information and a SAD module to assess the realism of concatenated super-resolved RGB image and predicted segmentation map. The AFE module takes the SR output and the GT HR as input to compute the feature loss \mathcal{L}_{fea} . The SAD module receives the concatenated pair to compute the segmentation-aware discrimination loss \mathcal{L}_D and the adversarial loss \mathcal{L}_{adv} . The SAD module is trained on the segmentation-aware discrimination loss \mathcal{L}_D . The entire network with SR and SS branches is jointly trained using the pixel-wise loss \mathcal{L}_2 , feature loss \mathcal{L}_{fea} , adversarial loss \mathcal{L}_{adv} and cross-entropy loss \mathcal{L}_{ce} .

improved accuracy compared to others at LR conditions, their gains remain marginal.

All of the aforementioned methods rely on inputs that are not extremely low resolution from the source and therefore retain substantial semantic content. Under our ULR setup, where available semantic information is severely constrained, these methods fail to produce satisfactory segmentation results as we show in our experiments. In this work, we aim to solve improved semantic segmentation generation from ULR RGB images, enabling semantic-based privacy-preserving downstream robotic tasks.

III. ULTRA-LOW-RESOLUTION SEMANTIC SEGMENTATION

We propose a novel joint-learning framework for ULR semantic segmentation. An overview of our framework is shown in Fig. 2. Given an ULR RGB input, we first employ a Generative Adversarial Network (GAN)-based SR network to reconstruct a high-resolution image. This super-resolution output is then passed through an encoder-decoder semantic segmentation network to produce improved segmentation map. We incorporate a agglomerative feature extractor (AFE) to extract high-level semantic features from the RGB representation. We concatenate the predicted segmentation map with the super-resolved RGB output, the GT segmentation with the HR RGB, and design a segmentation-aware discriminator (SAD) to assess the realism of both the generated HR RGB image and their predicted semantic segmentation map. The SAD module is trained separately with the segmentation-aware discrimination loss \mathcal{L}_D of the concatenated pair. Our

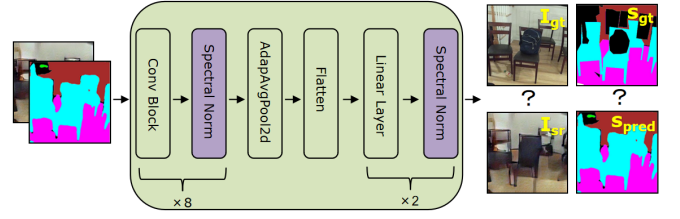


Fig. 3: Proposed segmentation-aware discriminator network architecture. The SAD module receives the concatenated pair of RGB image and semantic label and outputs the possibility of the generated RGB and its predicted label being judged as "real". The conv block consists of two sets of stacked 3×3 convolutional layers, followed by a spectral normalization layer (purple). The block output is then passed through an AdaptiveAvgPool2d and flattened into a one-dimensional representation. This vector is projected to a linear layer and subsequently regularized by spectral normalization.

proposed joint-learning method is trained on four losses: a pixel-wise difference between HR and super-resolved signal \mathcal{L}_2 , a feature loss \mathcal{L}_{fea} , an adversarial loss on the concatenated pair \mathcal{L}_{adv} and a pixel-wise cross-entropy loss \mathcal{L}_{ce} between the predicted label and the ground-truth (GT) label.

A. Joint-Learning Architecture

Considering the real-time constraints of robotic applications and the quality of super-resolution for segmentation, we adopt the standard ESRGAN generator built upon Residual-in-Residual Dense Network (RRDN) architecture proposed by Wang *et al.* [24]. Our implementation includes 23 residual-in-residual dense blocks (RRDBs), each RRDB encapsulating three dense blocks, and each dense block in turn consisting of five sub-layers (ConvBlocks).

We employ DeepLabV3+ [4] as the semantic segmentation module of our proposed end-to-end fully joint-learning framework. This method follows an encoder-decoder design. For the encoder, we use a pretrained ResNet-101 backbone to extract rich, multi-level feature maps, which are then passed to an Atrous Spatial Pyramid Pooling (ASPP) module to aggregate contextual information at multiple scales without reducing spatial resolution. The decoder upsamples the ASPP output, merges it with low-level encoder features to recover fine edges, applies a 3×3 refinement convolution, and restores full-resolution predictions through a second upsample.

The total loss is the balanced combination of SR and semantic segmentation, with α controlling the influence of each loss function.

$$\mathcal{L}_{tot} = (1 - \alpha) (\lambda_1 \mathcal{L}_2 + \lambda_2 \mathcal{L}_{fea} + \lambda_3 \mathcal{L}_{adv}) + \alpha \mathcal{L}_{ce} \quad (1)$$

For the super-generation part, we utilize a \mathcal{L}_2 pixel-wise reconstruction term as shown in Eq. (2), combined with a feature loss and a adversarial loss. The scalar coefficients λ controls the impact of each term.

$$\mathcal{L}_2 = \frac{1}{HWC} \sum_{h=1}^H \sum_{w=1}^W \sum_{c=1}^C (I_{gt}(h, w, c) - I_{sr}(h, w, c))^2 \quad (2)$$

where H, W, C are the height, width and channel dimensions of the image. I_{gt} and I_{sr} represent the GT and super-resolved

RGB image respectively. The details of feature loss \mathcal{L}_{fea} and extended adversarial loss \mathcal{L}_{adv} are provided in Sec. III-B and Sec. III-C respectively.

We employ the pixel-wise cross-entropy loss for semantic segmentation, which shows in Eq. (3):

$$\mathcal{L}_{ce}(x, y) = -x_y + \log \sum_j e^{x_j} \quad (3)$$

where x represents the raw logits and y is the ground-truth class index. The term x_y refers to the logit corresponding to the true class, while x_j denotes the logits for class j . This loss computes the negative log-likelihood of the correct class by implicitly applying a log-softmax operation.

B. Agglomerative Feature Extractor

Conventional GAN-based super-resolution networks calculate a perceptual loss by feeding the generated and ground truth RGB images to a pretrained network (VGG-16/19) [19]. However, when operating on the ULR inputs, the severely degraded textures and details render VGG-based perceptual guidance unsatisfactory. To better extract the semantic features for segmentation under ULR settings, we utilize the priors from large pretrained feature extraction model. In particular, we use RADIOv2.5-g version of AM-RADIO [15], which consolidates multiple large vision foundation models into a single, efficient student network as our feature extractor. As the module is required only during the training phase, it does not influence the real-time requirements of robotic applications.

We propose a feature loss, which combines a \mathcal{L}_1 loss and cosine-similarity \mathcal{L}_{cos} term:

$$\mathcal{L}_{fea} = \mathcal{L}_1 + \mathcal{L}_{cos} \quad (4)$$

$$\mathcal{L}_1 = \|\hat{F}_{real} - \hat{F}_{fake}\|_1 \quad (5)$$

$$\mathcal{L}_{cos} = 1 - \cos(\hat{F}_{real}, \hat{F}_{fake}) \quad (6)$$

The \mathcal{L}_1 component penalizes element-wise deviations to reinforce local detail consistency, while the cosine component aligns feature directions to improve global semantic coherence. By uniting these complementary objectives, our loss achieves more holistic feature alignment, thereby facilitating downstream semantic segmentation and improving the model generalization ability.

\hat{F} denotes the feature representation after \mathcal{L}_2 normalization, which is used to compute the angle.

C. Segmentation-Aware Discriminator

The key component of our approach is the Segmentation-Aware Discriminator, shown in Fig. 3 which extends the conventional GAN discriminator. A standard discriminator evaluates the visual fidelity between generated and ground-truth RGB images and primarily encourages the generator to produce images closely resembling the GT RGB, rather than images optimized for downstream task of semantic segmentation task. Under ULR conditions, where semantic information is severely limited, this exclusive focus on RGB

reconstruction does not lead to improved segmentation performance. In contrast, inspired by [22], which introduces segmentation cues to discriminator, our SAD module overcomes this limitation by jointly assessing both RGB reconstruction quality and segmentation accuracy, thereby balancing the adversarial reconstruction loss with a segmentation-driven objective to encourage the generator to produce outputs that are beneficial for semantic segmentation.

We introduce a segmentation-aware discrimination loss to train SAD:

$$\mathcal{L}_D = \mathcal{L}_{BCE}(\mathcal{D}(z_{real}), 1) + \mathcal{L}_{BCE}(\mathcal{D}(z_{fake}), 0) \quad (7)$$

$$\mathcal{L}_{BCE}(x, y) = -[y \log(\sigma(u)) + (1 - y) \log(1 - \sigma(u))] \quad (8)$$

$$\sigma(u) = \frac{1}{1 + e^{-u}}, \quad u \in \{\mathcal{D}(z_{real}), \mathcal{D}(z_{fake})\} \quad (9)$$

$$z_{real} = \text{concat}(I_{gt}, S_{gt}), \quad z_{fake} = \text{concat}(I_{sr}, S_{pred}) \quad (10)$$

Instead of using the relativistic discrimination loss from ESRGAN, we employ the binary cross-entropy (BCE) loss from SRGAN [10] for the discriminator, which estimates the probability that one input image comes from the true HR data distribution. Here $\mathcal{D}(\cdot)$ outputs the discriminator logits. z_{real} denotes the concatenated GT image I_{gt} with its segmentation mask S_{gt} while z_{fake} is the concatenated SR image I_{sr} with corresponding predicted semantic label S_{pred} .

The adversarial loss \mathcal{L}_{adv} derived from SAD in the total loss Eq. 1 is:

$$\mathcal{L}_{adv} = \mathcal{L}_{BCE}(\mathcal{D}(z_{fake}), 1) \quad (11)$$

Moreover, we employ spectral normalization [12] to scale the weights of SAD and guarantee Lipschitz-continuity. We discover this to be essential in improving GAN training stability. By bounding the gradients of SAD, it prevents large spikes in the backpropagation signal of generator and reduces the risk of instability.

IV. EXPERIMENTAL RESULTS

In this section, we validate the performance of our proposed method. Firstly, the experimental setup and implementation details are described. Then, the experimental results on SUN RGB-D dataset [20] are analyzed, followed by an ablation study. Subsequently, we investigate the relationship between the super-resolution module and ULR semantic segmentation. Finally, we analyze the zero-shot domain generalization capability of our proposed method on a custom real-world indoor dataset and evaluate its success rate in semantic object-goal navigation tasks under privacy-constrained conditions.

A. Setup

1) *Dataset*: We trained our network on the SUN RGB-D dataset [20], a widely used indoor semantic segmentation benchmark comprising 10,335 images across diverse indoor environments (offices, bedrooms, kitchens, etc.). Each image was cropped to 384×384 pixels to serve as our high-resolution ground truth. We randomly split the dataset into

Type	Method-label	Network-Architecture	SR-Trained	Seg-Trained	Training Dataset
Pretrained Pipeline	PP-1 [4]	DeepLabv3+	–	✓	384→384
	PP-2 [3]		×	✓	
Mono-Module Training	MMT-1 [13]	ESRGAN + Deeplabv3+	×	✓	16→384
	MMT-2 [6]		✓	×	
Fully Joint-Learning	FJL-1 [13]	ESRGAN + Deeplabv3+ + SAD + AFE	✓	✓	
	Ours		✓	✓	

TABLE I: Detailed configuration of each approach. Three types, in total five baselines and our proposed method are illustrated. Each method is represented by a concise method-label, which distinguishes differences in network-architecture, module training, and the training dataset resolutions. 384 → 384 and 16 → 384 represent that only the RGB inputs are processed to resolution of 384 and 16, but the segmentation outputs are always generated with 384.

Method	PP-1	PP-2	MMT-1	MMT-2	FJL-1	Ours
mIoU	0.0716	0.1241	0.2652	0.1640	0.2654	0.3101

TABLE II: Semantic segmentation test on 16×16 images of the SUN RGB-D dataset. Our proposed method achieves the highest semantic segmentation performance among all baselines.

a training set (9,000 images), a validation set (668 images), and a test set (667 images). To better train different methods, we processed the dataset into two groups of resolutions: 384 → 384 and 16 → 384.

2) *Training Setup*: Training was conducted on two NVIDIA A100 GPUs with a batch size of 16, and we evaluated our approach on a laptop equipped with an Intel i7-14650HX CPU. We set the training hyperparameters as follows: $\lambda_1 = 0.5$, $\lambda_2 = 0.01$, $\lambda_3 = 0.01$ and $\alpha = 0.3$. We adopted a two-stage training procedure, where we first pretrained the SR model using the original ESRGAN [24] losses: a pixel-wise MAE loss, a vanilla adversarial loss, and a VGG-based perceptual loss. This strategy accelerated convergence and mitigated the early-stage instabilities. In the second stage, we integrated the DeepLabv3+ segmentation network [4] and jointly trained both modules. Both stages used the same learning rate of $1e-4$ and employed ADAM optimizer with $\beta_1 = 0.9$ and $\beta_2 = 0.999$. We trained the model for 100 epochs and selected the best model according to the highest mean Intersection-over-Union on validation set.

3) *Evaluation Metrics*: We evaluate the mean Intersection-over-Union (mIoU) [4], which measures segmentation accuracy by computing the intersection divided by the union between predicted and GT segmentation regions across all classes.

4) *Baselines*: To assess the segmentation performance of our approach, we compare our proposed method against three categories of baselines: pretrained pipelines (PP), mono-module training (MMT), and fully joint-learning (FJL). Specifically, the following baselines are used:

- *PP-1* [4] uses a DeepLabv3+ segmentation network trained on the SUN RGB-D dataset at 384×384 resolution.
- *PP-2* [3] leverages a pretrained ESRGAN SR model combined with PP-1.
- *MMT-1* [13] trains exclusively segmentation network at ULR without training the SR module, which upsamples the ULR RGB images from 16×16 to 384×384 using bicubic interpolation.
- *MMT-2* [6] trains only the super-resolution network on

Method	Ours w/o SAD & w/o AFE (VGG-19)	Ours w/o SAD	Ours w/o AFE	Ours
mIoU	0.2713	0.2824	0.3021	0.3101

TABLE III: Module ablation on SUN RGB-D dataset at 16×16 resolution. Our proposed method with complete modules attains the highest mIoU, whereas removing either the SAD, or the AFE, or both modules (default VGG-19 loss) leads to a performance drop.

ULR inputs, with the segmentation network remaining frozen.

- *FJL-1* [13] jointly trains super-resolution and segmentation model on ULR inputs.

Further detailed information about the different baselines and our method is provided in Table I.

B. Ultra-Low-Resolution Semantic Segmentation Results

For comparison, we conducted an additional experiment using **full-resolution** (384×384) RGB inputs. In this setting, DeepLabv3+ achieves an mIoU of 0.4194, representing the upper-bound performance.

As demonstrated in Table II, at the ULR of 16×16 , our proposed method attains the highest mIoU, outperforming all baseline approaches. Applying a segmentation network pretrained on full-resolution inputs directly to 16×16 images (PP-1) causes the mIoU decrease dramatically from 0.4194 to 0.0716, highlighting the severe resolution sensitivity of this task. Although other baselines incorporate SR priors to enhance semantic segmentation performance, the highest mIoU achieved is 0.2654, still far from the full-resolution result (0.4194), indicating that conventional SR networks cannot directly benefit semantic segmentation. As can be seen, our proposed method surpasses the best-performing baseline (FJL-1) by 16.84%, demonstrating that our adjusted SR effectively facilitates ULR semantic segmentation.

C. Ablation Study

In this section, we conduct an ablation study of our method on ULR 16×16 setting. We test semantic segmentation performance of our proposed method on the SUN RGB-D test set after separately removing segmentation-aware discriminator and agglomerative feature extractor as demonstrated in Table III. Regardless of which core module is removed, the mIoU score of our proposed method drops. Removing both modules and relying solely on the default perceptual loss from VGG-19 results in a mIoU drop to 0.2713, highlighting that both modules are important for ULR semantic segmentation. Specifically, removing the SAD

Method	PSNR \uparrow	SSIM \uparrow	LPIPS \downarrow	FID \downarrow	ARI \uparrow	Covering \uparrow	BF \uparrow	mIoU \uparrow
PP-1	20.03	0.6124	0.7088	263.78	0.1220	0.3666	0.0514	0.0716
PP-2	20.02	0.5598	0.5631	218.27	0.1477	0.3831	0.0906	0.1241
MMT-1	20.03	0.6124	0.7088	263.78	0.3462	0.4934	0.1374	0.2652
MMT-2	15.91	0.4382	0.5151	104.43	0.2885	0.4540	0.1303	0.1640
FJL-1	12.22	0.3218	0.5839	100.94	0.3524	0.4917	0.1452	0.2654
Ours	15.07	0.4059	0.4892	242.73	0.4010	0.5271	0.1359	0.3101

TABLE IV: Qualitative comparison of super-resolution outputs, segmentation and semantic segmentation results. Given the ultra-low-resolution 16×16 inputs, we compare five baselines and our proposed approach. As shown in the table, our method achieves the highest values in semantic segmentation (mIoU) as well as segmentation ARI and Covering, demonstrating the best overall segmentation performance, despite not obtaining the strongest RGB reconstruction metrics. This indicates that segmentation accuracy is not directly positively correlated with RGB image quality.

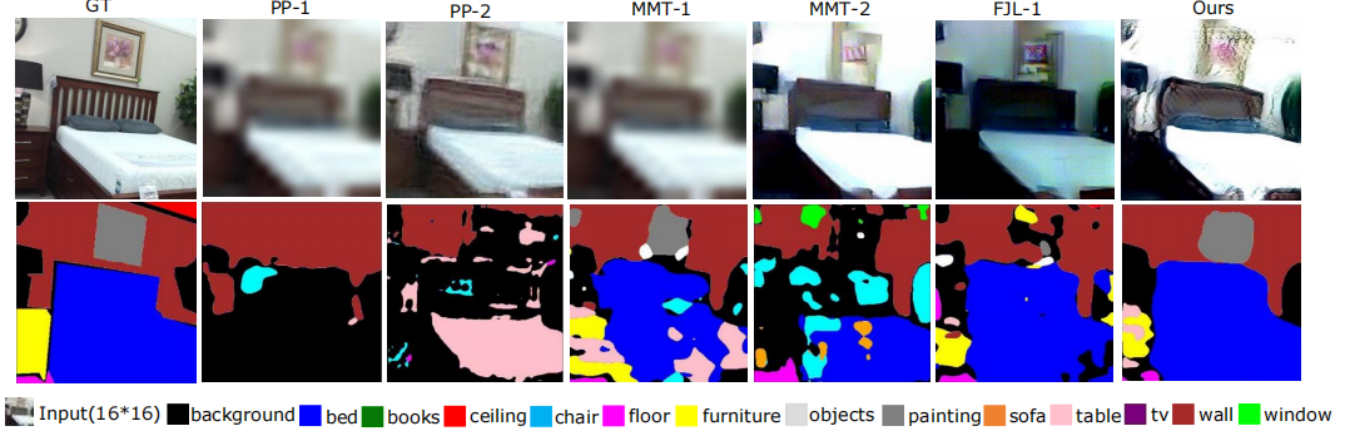


Fig. 4: Visual comparison of super-resolution RGB images and semantic segmentation maps. We compare the visualization results of super-resolved outputs and predicted semantic-segmentation produced by five baselines and our proposed method against the GT, under setting of 16×16 input. Our method produces the most accurate semantic segmentation compared to all baselines, despite generating RGB images of lower visually quality. Our method amplifies object-boundary contrast to favor region delineation, and achieves best semantic segmentation accuracy at the expense of boundary segmentation.

module reduces mIoU to 0.2824, with 9.8% less, indicating that SAD is essential for guiding the generator to produce SR images that are beneficial for semantic segmentation. While the AFE underscores the importance of extracted high-level features for robust segmentation when input information is severely limited.

D. Analysis Between Super-Resolution and Ultra-Low-Resolution Semantic Segmentation

Building on our findings in Sec. IV-B, a natural question arises: Does super-resolution really help for ultra-low-resolution semantic segmentation? To better understand why our proposed method helps ULR semantic segmentation effectively, we calculated the metrics for the intermediate super-resolved RGB images and their corresponding segmentation outputs in Table IV, and visualized the results in Fig. 4. Our proposed pipeline outputs only semantic segmentation maps, without generating or storing intermediate super-resolved images. The intermediate super-resolved results shown here in Fig. 4 are solely for visualization purposes to facilitate analysis of the relationship between super-resolution and ULR-based semantic segmentation, and thus do not raise privacy concerns. Specifically, to assess the RGB reconstruction fidelity, we employ four widely used image-quality metrics: Peak Signal-to-Noise Ratio (PSNR), Structural Similarity Index Measure (SSIM), Learned Per-

ceptual Image Patch Similarity (LPIPS) and Fréchet Inception Distance (FID) [9]. For the evaluation of segmentation accuracy, we report two region-based indices, Adjusted Rand Index (ARI), Segmentation Covering (Covering), and one boundary-based metric, Boundary F-measure (BF) [2], and one overall semantic segmentation metric mIoU.

As shown in Table IV, we observed three interesting findings:

- Under ULR conditions, standard super-resolution models do not directly improve downstream semantic segmentation.
- Under ULR conditions, higher PSNR and SSIM do not necessarily lead to better segmentation performance. Both PP-1 and MMT-1 upscale 16×16 inputs to the full-resolution size (384×384) via bicubic interpolation, achieving the highest PSNR and SSIM among all methods. However, their segmentation results remain unsatisfactory. In contrast, FJL-1 generates RGB images with lower PSNR and SSIM, yet its semantic segmentation results are quite close to MMT-1.
- Under ULR conditions, lower LPIPS and FID do not guarantee better segmentation performance. Although MMT-2 produces outputs that are perceptually (LPIPS) and distributionally (FID) closer to the ground truth, its segmentation accuracy lags behind to that of MMT-1.

Method	PP-1	PP-2	MMT-1	MMT-2	FJL-1	Ours
mIoU	0.0576	0.1330	0.2508	0.1650	0.2391	0.3177

TABLE V: Semantic segmentation test on 16×16 images of our custom real-world dataset. Our method achieves the best zero-shot domain generalization semantic segmentation performance among all baselines.

Our proposed method generates intermediate super-resolved RGB images with lower image quality and color discrepancies compared to the ground truth. However, by compromising RGB reconstruction fidelity, our approach prioritizes generating images that are optimally tailored for semantic segmentation. As a result, our method attains the best performance in region-based segmentation, and delivers the highest overall semantic segmentation performance. As illustrated in Fig 4, despite the visual differences between our generated RGB images and the ground truth, our approach enhances inter-object region distinctions, thus effectively facilitating semantic segmentation. Nevertheless, our approach yields a lower BF score, this might be due to color bleeding at object boundaries, which broadens the edge regions. We leave this as an open question and our future work.

We validate that a standard super-resolution module alone does not directly help segmentation performance. While our proposed approach, incorporating segmentation cues into the discriminator and leveraging priors from a large pretrained feature extractor, effectively enhances accuracy.

E. Zero-shot Domain Generalization

To assess the zero-shot domain generalization capability of our method, i.e., without any fine-tuning on the new dataset, we further created a custom small-scale indoor dataset comprising 90 annotated RGB and semantic segmentation pairs, following the data collection scheme of the NYU Depth V2 [18] dataset. We conducted this domain generalization test before deploying it in a real-world navigation task, to preliminarily evaluate our method’s applicability and generalization, thereby reducing the resources expenditure.

Table V shows the semantic segmentation results on our custom indoor-scene dataset under the ULR setting (16×16). Our method achieves the highest mIoU among all the approaches, representing a substantial improvement of 26.67% over the strongest baseline (MMT-1). This result closely matches our performance on the SUN RGB-D test set, demonstrating the robustness of our approach and its strong zero-shot domain generalization ability at ULR conditions.

F. Privacy-Preserving Semantic Object-Goal Navigation

Object-goal navigation, the task of enabling a robot to locate and approach a specified object within unknown environments, has become essential in robotics [21]. A widely adopted strategy leverages semantic information [26] to facilitate object-level navigation. We applied semantic object-goal navigation to showcase that it preserves privacy using only ULR RGBs as inputs and enables navigation functionality through improved semantic segmentation outputs.

Our system comprises three modules. Given a target object, the robot first starts the *Semantic Coverage* module.

Method	FJL-1	MMT-1	Ours
Success Rate (%)	62.5	65.0	85.0

TABLE VI: Privacy-preserving semantic object-goal navigation success rate. We conducted a total of 40 trials, testing four target objects from two distinct starting locations. Our proposed method achieves the highest navigation success rate, surpassing MMT-1 and FJL-1. Thus, our improved ULR semantic segmentation results increase the success rate of object-goal navigation in real-world scenarios with privacy constraints.

If the target object is found, the robot switches to the *Object Goal Navigation* module to approach it. If the target object is not segmented, our system calls the *Floor Based Navigation* module to determine the next best waypoint for exploration. We randomly sample midpoints at fixed intervals to define the robot’s movement waypoints. Foreground pixels deviating horizontally from fitted boundary lines beyond a threshold are identified as branch points, indicating potential new area entrances. If no further waypoint is available, our system concludes that the target object is not found. Otherwise, the robot moves to the new waypoint, and the loop continues.

We deployed the approaches in a real-world indoor environment as shown in Fig. 1. The experiments were conducted using the OrionStar GreetingBot Mini¹ mobile robot, with only the onboard RGB camera activated for perception. ULR images are simulated by downsampling full-resolution images to 16×16 using bicubic interpolation. To further validate our findings in Sec. IV-B and Sec. IV-E, we compare our proposed method against the best baselines on SUNRGB-D and custom dataset in the real world. We conducted experiments using four target objects: sofa, chair, table, and painting. For each object, the robot is initialized from two starting locations: one in the corridor and the other inside the room. Each object-starting point pair is tested five times, resulting in a total of 40 trials. The success rate is used for evaluation and computed as the proportion of trials in which the robot successfully navigates from the starting location to the target object. A success trail is defined when the segmented pixels of the target object occupy more than 40% of the image.

From the results shown in Table VI, our method achieves the highest navigation success rate compared to other baselines, outperforming MMT-1 and FJL-1 by 20 and 22.5 percentage points respectively. Under a privacy-constrained scenario using only ULR RGB images as inputs, our improved ULR semantic segmentation results increase the success rate of the semantic object-goal navigation. To further illustrate how improved mIoU contributes to improved navigation, we present semantic segmentation results across two consecutive frames in Fig. 5. These results demonstrate that successful navigation toward a target object requires consistently accurate segmentation across frames. Our method yields more stable and coherent segmentation results, whereas MMT-1 and FJL-1 fail to maintain correct segmentation in consecu-

¹<https://en.orionstar.com/mini.html>

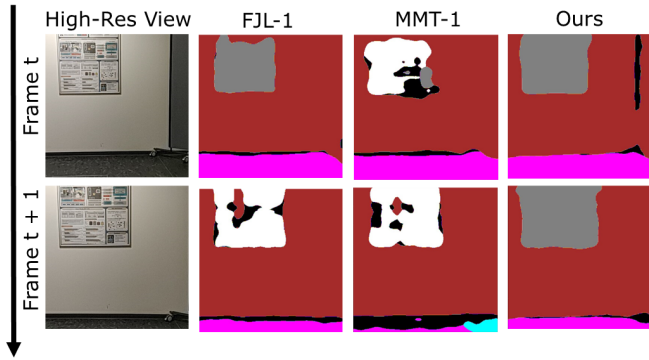


Fig. 5: Semantic segmentation results during navigation across two consecutive frames. The first row shows the high-resolution image for visualization at time step t and its corresponding segmentation outputs from FJL-1, MMT-1, and our method. The second row presents the results for the subsequent frame ($t+1$). Compared to baselines, our method yields more stable and consistent segmentation across frames, enabling successful navigation by continuously segmenting the target object. In contrast, MMT-1 and FJL-1 exhibit segmentation failures in the subsequent frame, which leads to navigation failure to the target object.

tive frames, ultimately causing the robot to miss the target.

V. CONCLUSION

In this paper, we present a novel joint-learning framework that recovers HR semantic segmentation maps from only ULR RGB inputs. The proposed method combines a segmentation-aware discriminator and an agglomerative feature extractor to address loss imbalance and semantic feature extraction limitation at ULR conditions. Our experiments demonstrate that, under ULR scenarios, our approach outperforms different types of strong baselines in semantic segmentation accuracy. We validate that conventional super-resolution network in existing baselines fails to directly improve segmentation in ULR setup, whereas our integration of segmentation guidance and large pretrained feature extraction priors can improve semantic segmentation performance effectively under ULR settings. Moreover, our proposed method shows zero-shot domain generalization and enables privacy-preserving robotic applications such as semantic object-goal navigation. Our experiments demonstrate that improving ULR semantic segmentation leads to a higher success rate in semantic object-goal navigation under real-world privacy-constrained conditions.

ACKNOWLEDGMENT

We gratefully acknowledge Liren Jin for the insightful discussions and invaluable assistance throughout this work.

APPENDIX

As discussed earlier, some users consider that RGB images with 32×32 resolution can meet their basic privacy needs [7]. Here we also evaluated the performance of our proposed method at a resolution of 32×32 . Table VII shows the semantic segmentation results of our method and different baselines. Our proposed method still achieves the highest mIoU compared to other baselines. Since the performance

mIoU	PP-1	PP-2	MMT-1	MMT-2	FJL-1	Ours-32
Value	0.1514	0.2389	0.3580	0.2951	0.3832	0.3991

TABLE VII: Semantic segmentation test on 32×32 images of the SUN RGB-D dataset. MMT-1, MMT-2, FJL-1 and Ours-32 are trained on $32 \rightarrow 384$ dataset. Our proposed method outperforms all baselines in semantic segmentation at 32×32 , attaining the highest mIoU.

gap between our proposed method at 32×32 and the full-resolution result (0.4194) is minimal, we focus our work on the more challenging 16×16 ULR setting, which fully guarantees the user privacy.

REFERENCES

- [1] G. K. Alshammari, A. Abubakar, N. M. Ahmed, and N. K. Alshammari, "Federated Learning-based Semantic Segmentation for Lane and Object Detection in Autonomous Driving," *arXiv preprint arXiv:2504.18939*, 2025.
- [2] P. Arbelaez, M. Maire, C. Fowlkes, and J. Malik, "Contour detection and hierarchical image segmentation," *IEEE Trans. on Pattern Analysis and Machine Intelligence (PAMI)*, 2010.
- [3] J. Caputa, M. Wielgosz, D. Łukasik, P. Russek, J. Grzeszczyk, M. Karwowski, S. Mazurek, R. Frączek, A. Śmiech, E. Jamro *et al.*, "Using super-resolution for enhancing visual perception and segmentation performance in veterinary cytology," *Journal of Life (Life)*, 2024.
- [4] L.-C. Chen, Y. Zhu, G. Papandreou, F. Schroff, and H. Adam, "Encoder-decoder with atrous separable convolution for semantic image segmentation," in *Proc. of the Europ. Conf. on Computer Vision (ECCV)*, 2018.
- [5] M. M. Coffer, "Balancing privacy rights and the production of high-quality satellite imagery," 2020.
- [6] T. Frizza, D. G. Dansereau, N. M. Seresht, and M. Bewley, "Semantically accurate super-resolution generative adversarial networks," *Journal of Computer Vision and Image Understanding (CVIU)*, vol. 221, 2022.
- [7] X. Huang, S. Pan, and M. Bennewitz, "Privacy risks of robot vision: A user study on image modalities and resolution," *arXiv preprint arXiv:2505.07766*, 2025.
- [8] M. U. Kim, H. Lee, H. J. Yang, and M. S. Ryoo, "Privacy-preserving robot vision with anonymized faces by extreme low resolution," in *Proc. of the IEEE/RSJ Intl. Conf. on Intelligent Robots and Systems (IROS)*, 2019.
- [9] Y. Kong and S. Liu, "Dmsc-gan: A c-gan-based framework for super-resolution reconstruction of sar images," *Remote Sensing*, 2023.
- [10] C. Ledig, L. Theis, F. Huszár, J. Caballero, A. Cunningham, A. Acosta, A. Aitken, A. Tejani, J. Totz, Z. Wang *et al.*, "Photo-realistic single image super-resolution using a generative adversarial network," in *Proc. of the IEEE/CVF Conf. on Computer Vision and Pattern Recognition (CVPR)*, 2017.
- [11] Z. Liu, H. Zhu, R. Chen, J. Francis, S. Hwang, J. Zhang, and J. Oh, "Mosaic: Generating consistent, privacy-preserving scenes from multiple depth views in multi-room environments," *arXiv preprint arXiv:2503.13816*, 2025.
- [12] T. Miyato, T. Kataoka, M. Koyama, and Y. Yoshida, "Spectral normalization for generative adversarial networks," *arXiv preprint arXiv:1802.05957*, 2018.
- [13] M. B. Pereira and J. A. dos Santos, "An end-to-end framework for low-resolution remote sensing semantic segmentation," in *IEEE Latin American GRSS & ISPRS Remote Sensing Conference*, 2020.
- [14] M. Pietrantonio, M. Humenberger, T. Sattler, and G. Csurka, "Segloc: Learning segmentation-based representations for privacy-preserving visual localization," in *Proc. of the IEEE/CVF Conf. on Computer Vision and Pattern Recognition (CVPR)*, 2023.
- [15] M. Ranzinger, G. Heinrich, J. Kautz, and P. Molchanov, "Am-radio: Agglomerative vision foundation model reduce all domains into one," in *Proc. of the IEEE/CVF Conf. on Computer Vision and Pattern Recognition (CVPR)*, 2024.
- [16] D. Reinhardt, M. Khurana, and L. H. Acosta, "i still need my privacy": Exploring the level of comfort and privacy preferences of german-speaking older adults in the case of mobile assistant robots," *Journal of Pervasive and Mobile Computing (PMC)*, vol. 74, 2021.
- [17] M. Rueben and W. D. Smart, "Privacy in human-robot interaction: Survey and future work," *Proc. of the Intl. Conf. on We robot*, 2016.

- [18] N. Silberman, D. Hoiem, P. Kohli, and R. Fergus, "Indoor segmentation and support inference from rgb-d images," in *Proc. of the Europ. Conf. on Computer Vision (ECCV)*, 2012.
- [19] K. Simonyan and A. Zisserman, "Very deep convolutional networks for large-scale image recognition," *arXiv preprint arXiv:1409.1556*, 2014.
- [20] S. Song, S. P. Lichtenberg, and J. Xiao, "Sun rgb-d: A rgb-d scene understanding benchmark suite," in *Proc. of the IEEE/CVF Conf. on Computer Vision and Pattern Recognition (CVPR)*, 2015.
- [21] J. Sun, J. Wu, Z. Ji, and Y.-K. Lai, "A survey of object goal navigation," *IEEE Trans. on Automation Science and Engineering (TASE)*, 2024.
- [22] V. Sushko, E. Schönfeld, D. Zhang, J. Gall, B. Schiele, and A. Khoreva, "You only need adversarial supervision for semantic image synthesis," in *Proc. of the Intl. Conf. on Learning Representations (ICLR)*, 2021.
- [23] A. K. Taras, N. Suenderhauf, P. Corke, and D. G. Dansereau, "The need for inherently privacy-preserving vision in trustworthy autonomous systems," *arXiv preprint arXiv:2303.16408*, 2023.
- [24] X. Wang, K. Yu, S. Wu, J. Gu, Y. Liu, C. Dong, Y. Qiao, and C. Change Loy, "Esrgan: Enhanced super-resolution generative adversarial networks," in *Proceedings of the European conference on computer vision (ECCV) workshops*, 2018.
- [25] M. Xu, M. Islam, L. Bai, and H. Ren, "Privacy-preserving synthetic continual semantic segmentation for robotic surgery," *IEEE Trans. on medical imaging (TMI)*, 2024.
- [26] N. Yokoyama, S. Ha, D. Batra, J. Wang, and B. Bucher, "Vlfn: Vision-language frontier maps for zero-shot semantic navigation," in *Proc. of the IEEE Intl. Conf. on Robotics & Automation (ICRA)*, 2024.